




Article

Approach to Hybrid Energy Storage Systems Dimensioning for Urban Electric Buses Regarding Efficiency and Battery Aging

Jorge Nájera ^{1,*} , Pablo Moreno-Torres ², Marcos Lafoz ³ , Rosa M. de Castro ¹ and Jaime R. Arribas ¹ 

¹ Department of Electrical Engineering, E.T.S.I. Industriales, Universidad Politécnica de Madrid, 28006 Madrid, Spain; rosamaria.decastro@upm.es (R.M.d.C.); jaime.rodriguez@upm.es (J.R.A.)

² Wynnertech S.L., 28906 Madrid, Spain; pmorenortorres@wynnertech.es

³ CIEMAT, Government of Spain, 28040 Madrid, Spain; marcos.lafoz@ciemat.es

* Correspondence: jorge.najera.alvarez@alumnos.upm.es; Tel.: +34-628-711-054

Received: 28 September 2017; Accepted: 23 October 2017; Published: 26 October 2017

Abstract: This paper focuses on Hybrid Energy Storage Systems (HESS), consisting of a combination of batteries and Electric Double Layer Capacitors (EDLC), for electric urban busses. The aim of the paper is to develop a methodology to determine the hybridization percentage that allows the electric bus to work with the highest efficiency while reducing battery aging, depending on the chosen topology, control strategy, and driving cycle. Three power electronic topologies are qualitatively analyzed based on different criteria, with the topology selected as the favorite being analyzed in detail. The whole system under study is comprised of the following elements: a battery pack (LiFePO₄ batteries), an EDLC pack, up to two DC-DC converters (depending on the topology), and an equivalent load, which behaves as an electric bus drive (including motion resistances and inertia). Mathematical models for the battery, EDLCs, DC-DC converter, and the vehicle itself are developed for this analysis. The methodology presented in this work, as the main scientific contribution, considers performance variation (energy efficiency and battery aging) and hybridization percentage (ratio between batteries and EDLCs, defined in terms of mass), using a power load profile based on standard driving cycles. The results state that there is a hybridization percentage that increases energy efficiency and reduces battery aging, maximizing the economic benefits of the vehicle, for every combination of topology, type of storage device, control strategy, and driving cycle.

Keywords: battery aging; electric bus; energy efficiency; Hybrid Energy Storage

1. Introduction

The huge impact that transportation has on greenhouse gas emissions is well known. According to the US Environmental Protection Agency (EPA), around 26% of the total greenhouse gas emissions are caused by transports, and, from that percentage, 22% corresponds to heavy vehicles like buses and freight trucks [1]. Transport electrification policies have been applied, for instance, by the European Union, with the objective of reducing transportation emissions, and, in fact, this is one of the key research areas of the Horizon2020 European research programme [2]. Additionally, there are multiple European cities that are restricting the access of combustion engine vehicles to urban areas [3], which makes it even more crucial to electrify urban transportation in order to have livable and sustainable cities.

Energy storage systems (ESSs) are still the bottleneck for electric transportation and will keep being so for some time due to their low energy density and high cost. The electrical storage technologies used in Electric Vehicles (EVs) and Electric Buses (EB) [4,5] are one of the key issues to ensure this

development due to their driving range and manufacturing costs. Only a few technologies are applicable nowadays, namely batteries, fuel cells, and EDLCs.

EDLCs are high power density storage systems, while batteries and fuel cells compete against each other as they are both high energy density storage systems. At present, batteries are ahead in terms of Technology Readiness Level, Regulatory Readiness Level, and Customer Readiness Level [4–6]. Research on new battery chemistries such as lithium-metal, lithium-sulfur, or metal-air is promising and maybe optimistic as well. However, batteries are not exempt from drawbacks such as those related to thermal behavior and especially aging derived from the demanding power profile and the number of cycles required, which will strongly affect their life cycle.

Given that batteries and EDLCs provide complementary capabilities, the use of a combined solution of both technologies, known as a Hybrid Energy Storage System (HESS), seems to provide clear advantages. The synergy of using a combination of batteries and EDLCs provides potential for achieving better performance at the cost of higher complexity. This extra expertise requirement is probably one of the reasons why current commercial hybrid and electric buses still use either batteries or EDLCs as electrical ESS, although future electrical buses may evolve towards HESS, consisting of batteries and EDLCs together.

There are already many studies in the scientific literature that approach the topic of HESS for electrical transports from the topology, from the dimensioning, or from the control strategy point of view (e.g., [7,8]). However, there are not many works that consider two or more aspects simultaneously, and this is one of the contributions of this paper. A complete evaluation of the benefits, considering all parts of the equipment, is likely to reveal that the total efficiency during the life cycle of the EB can be increased.

This paper proposes a HESS dimensioning methodology that aims at getting a most favorable hybridization percentage, taking into consideration the control strategy and the driving cycle for a chosen HESS topology. For the studies carried out in this paper, the combined use of LiFePO₄ batteries and EDLCs for high power EBs is proposed, using the appropriate topology of a DC-DC power electronic converter. A qualitative study of three topologies is presented in Section 2, and the one deemed more appropriate, both technically and economically, is selected for the rest of the study. Models of LiFePO₄ batteries, EDLCs, and interleaved DC-DC converters are described in Section 3, highlighting the novelties proposed in this paper, together with the implemented control strategy. As an example of the application of the methodology proposed in this paper, these models are used in Section 4 to assess the performance of the whole HESS in terms of power losses, runtime (driving range), and battery aging for two different driving cycles. Finally, conclusions are drawn in Section 5.

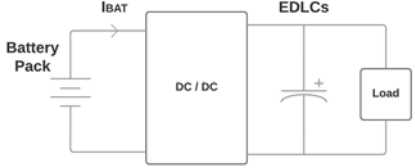

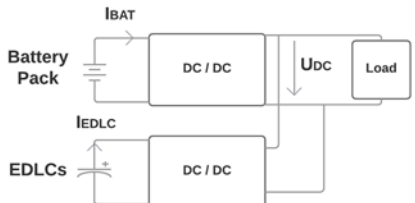
2. Topologies Used for HESS Integration

HESS for EVs and EB comprise two power sources (batteries and EDLCs) and one bidirectional load (the traction drive composed by the inverter, the traction motor, and the mechanical load). Using a combination of batteries and EDLCs, operating at different voltage allows the specific power and energy to be improved for each application since energy is mainly given by batteries and power by both batteries and EDLCs [9]. For such configuration, there are seven possible power topologies [5,7,9]. Out of those seven topologies, only the three represented in Table 1 have been taken into consideration since they provide the minimum control flexibility required and increase the reliability during their implementation in an EB.

In topology 1, “two-stage battery/EDLCs”, the DC-DC keeps batteries under control, which is preferable to the EDLCs as the former are more sensitive to extreme operation (high current, overdischarge, etc.). However, this advantage comes at the expense of the under-use of the EDLCs, as their voltage will most likely be constrained within a narrow range and the capability of the EDLCs to provide/absorb power peaks is reduced, which, in turn, places more demanding operating conditions on the batteries. The DC-DC converter must keep the DC-link voltage U_{DC} (which is also the EDLCs voltage) within a certain range by charging and discharging the batteries. This control

should allow U_{DC} to vary within a certain range so that the EDLCs are used as effectively as possible [8]. For example, a time-averaged load current is used as a current reference for the batteries in [10].

Table 1. The two-source one-load Hybrid Energy Storage Systems (HESS) boost topologies studied for this paper.

Topology	Controlled Variables	Schematic
1 Two-stage battery/EDLCs	I_{BAT}	
2 Two-stage EDLCs/battery	I_{EDLC}	
3 Parallel active	$U_{DC}/I_{BAT}/I_{EDLC}$	

Topology 2, “two-stage EDLCs/battery”, is probably the most studied one. The EDLCs voltage may vary in a wide range (usually from 40% to 50% to 100%, which implies using around 75% of their capacity). In addition, their rated voltage may be lower when compared to the previous topology. However, the converter needs to be of higher power than the one in topology 1 since, at lower EDLC voltage, the current demanded will be higher if a constant power supply is requested. Another limitation of this alternative is that the DC-link voltage U_{DC} cannot be varied as it is imposed by the battery pack [8]. The simplest way to control the system consists in rule-based strategies that cannot perform optimally [11,12]. Particularly interesting is the work presented in [13], in which three rule-based control strategies are tested with three different goals: optimal power split between the batteries and the EDLCs, loss minimization, and State of Charge (SoC) optimization. The study suggests that even a simple control strategy enables efficient energy savings (when compared to conventional non-hybrid ESSs), but the authors of the present work think that such a statement cannot be generalized, as is discussed later.

Topology 3, “parallel active”, has been receiving a lot of focus lately since it is arguably the most flexible topology for EBs applications. Indeed, it has flexible operating voltages and provides explicit power sharing control [5–7,9], although both currents are not independent since, when either I_{BAT} or I_{EDLC} is prioritized for control, the other one is set by the traction drive. There is no doubt that it is the only topology with inherent redundancy since the failure of one source does not prevent the operation of the other, which, in some applications, is an important specification. For the reasons stated above, this alternative is preferred in traction applications. However some authors argue against this topology due to the weight of two power converters [13] and the extra cost.

Each of the three possible topologies presents advantages and disadvantages in terms of voltage flexibility, control flexibility, control complexity, effective capacity utilization, the number and size of the DC-DC converters (including weight, volume, and cost), and system reliability and redundancy.

For the analysis carried out in Section 4, topology 2 has been chosen for the advantage of the combined storage technologies. Topology 1 was discarded since it has only one true ESS, as the

EDLCs behave like an improved DC-link. Topology 3 was discarded for weight, cost, and excessive complexity reasons.

3. HESS Modelling for Energy Efficiency and Battery Aging

The mathematical models used in the analysis carried out in Section 4 are described next. Three main devices are considered: a lithium-ion (LiFePO₄) battery pack, an EDLC pack, and a DC-DC power electronic converter. Obviously, the more accurate and complete the model is, the more information can be obtained from it. However, model parameters are usually rather difficult to determine, especially in the case of the battery, the non-linear dynamic model of which depends not only on the electrical and thermal variables but also on its lifetime and operation history [4,14,15].

3.1. Battery Model

3.1.1. Voltage-Current Performance and Runtime Model

The lithium-ion battery model used in this paper is a modification of the Mathworks model in the SimPower toolbox from Simulink [16]. The equivalent circuit is based on the Shepherd model [17], which was developed and experimentally validated later [18,19]. Although more accurate equivalent circuits have been proposed [20], the Shepherd model keeps the error between 1% and 5% and does not require testing the battery to obtain parameters (datasheet information suffices). In this paper, the battery model is based on the one described in [19] and behaves as follows:

$$E = f(\text{SoC}) = E_0 - K \times Q_{\text{MAX}} \left(\frac{100}{\text{SoC}} - 1 \right) + A \times e^{-B \cdot Q_{\text{MAX}} (1 - \frac{\text{SoC}}{100})} \quad (1)$$

$$R_{\text{POL},\text{discharge}} = f(\text{SoC}) = K \frac{100}{\text{SoC}} \quad (2)$$

$$R_{\text{POL},\text{charge}} = f(\text{SoC}) = K \frac{1}{1.1 - \frac{\text{SoC}}{100}} \quad (3)$$

where u is the battery instantaneous voltage [V], i is the battery current [A], $i > 0$ discharging; $i < 0$ charging, SoC is the battery state of charge [%], I_{SELF} is the self-discharge current [A], R_{OHM} is the ohmic internal resistance [Ω], R_{POL} is the polarization internal resistance [Ω], C_{POL} is the polarization capacitor [F], E is the open-circuit nonlinear voltage [V], E_0 is the open-circuit constant voltage [V], K is the polarization constant [Ah^{-1}], Q_{MAX} is the maximum capacity [Ah], A is the exponential voltage constant [V], and B is the exponential capacity constant [Ah^{-1}].

The model originally proposed in [19] considers the following assumptions: the parameters are the same for charging and discharging, the Peukert effect and memory effect are negligible, the internal resistance is constant, and the temperature does not affect the behavior of the battery. The model used in this paper differs from the one in [19] in that it loses generality for the sake of simplicity since it is only valid for lithium-ion batteries. In this work, the following modifications in the battery model have been introduced for the development of a new thermal model, explained in Section 3.1.2., “Thermal Model”:

- (1) Temperature dependencies are added to and implemented in the model used in this work, as shown in Figure 1.
- (2) Internal resistance is modelled as two different electrical resistances, ohmic resistance and polarization resistance, the latter being dependent on the SoC . Since ohmic resistance is almost constant over 20% to 100% SoC , its SoC dependency has not been considered [20].

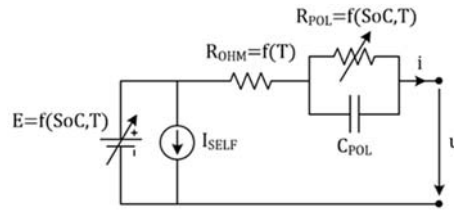


Figure 1. The battery equivalent circuit used in this work updated with temperature dependencies.

3.1.2. Thermal Model

Temperature is important when studying battery runtime and aging, but it also affects power losses and efficiency. Similarly, voltage also depends on temperature. Although the polarization time constant (given by C_{POL}) and self-discharge also change with temperature, neither of them are considered particularly relevant for the purposes of this work.

Considering temperature-dependent parameters implies modelling the thermal dynamics of the battery pack. The thermal model implemented is comprised of two parts: a heat generation model and a heat evacuation model. The first one was developed based on the work presented in [21]. Three heat sources or mechanisms are considered for lithium-ion batteries: irreversible heat (or reaction heat), reversible heat, and ohmic heat [22–24]:

$$H = (E_0 - E)i + T \frac{dE}{dT} i + (R_{OHM} + R_{POL})i^2 \quad (4)$$

where H is the heat generated, E is the cell voltage, $i > 0$ corresponds to the discharge, T [K] is the temperature, and $dE/dT \geq 0$ is the change of the equilibrium potential with temperature, which varies with SoC [23]. Other minor sources of heat such as side reactions accounting for aging are considered negligible for the purposes of this work [23].

In order to simplify the thermal model, dE/dT is assumed to be constant and greater than 0. The rest of the parameters (E_0 , Q_{MAX} , R_{POL} , R_{OHM}) are temperature dependent:

$$E_0(T) = E_0(T_0) + \frac{dE}{dT}(T - T_0) \quad (5)$$

$$Q_{MAX}(T) = Q_{MAX}(T_0) + \frac{dQ}{dT}(T - T_0) \quad (6)$$

$$K(T) = K(T_0) \times e^{\alpha(\frac{1}{T} - \frac{1}{T_0})} \quad (7)$$

$$R_{OHM}(T) = R_{OHM}(T_0) \times e^{\beta(\frac{1}{T} - \frac{1}{T_0})} \quad (8)$$

The second part of the thermal model represents the heat evacuation, both within a single cell and for a whole battery pack. As this part highly depends on the specific EB design under analysis (particularly on those aspects regarding the battery pack and its cooling system), a simplified approach has been taken in this work regarding the whole pack. Namely, it is assumed that both the heat generation and the internal temperature of the cell are constant and uniform, which is a reasonable approximation according to [25]. This implies that the only heat transfer to be modelled is that from the cell surface to the ambient. Strictly speaking, this heat transfer uses two mechanisms, convection and radiation. However, the latter is negligible in this case, which yields the following energy balance equation [22]:

$$H \approx m \cdot c_p \frac{dT}{dt} + \frac{1}{R_{OUT}}(T - T_0) + E \times \sigma \times (T^4 - T_0^4) \Rightarrow R_{OUT} = \frac{1}{h \cdot Ar} \quad (9)$$

where m and c_p [$\text{J} \cdot \text{kg}^{-1} \cdot \text{K}^{-1}$] are the mass and the specific heat capacity of the cell, h [$\text{W} \cdot \text{m}^{-2} \cdot \text{K}^{-1}$] is the convective heat transfer coefficient, and Ar is the external surface area of one cell. The variation in temperature over time for a single cell is given by:

$$T(s) = \frac{H \times R_{OUT} + T_0}{1 + m \times c_p \times R_{OUT} \times s} = \frac{H \cdot R_{OUT} + T_0}{1 + t_{th} \times s} \quad (10)$$

where t_{th} [s] is a thermal time constant.

Once a single cell has been modelled from the thermal point of view, there is the question of how to deal with a whole battery pack. Based on the results provided in [26], the following approximate law was deduced and implemented in the present work:

$$R'_{OUT}(N_s) = \sqrt[6]{\frac{N_s}{2}} \times R_{OUT} \quad (11)$$

where N_s is the number of cells in series. Note that R'_{OUT} affects both the steady-state temperature of the cell and the time needed to reach steady-state, increasing both of them.

3.1.3. Aging Model

Battery aging has also been included in the model developed during this paper for cycle life estimation purposes. The aging of lithium-ion cells has already been studied, and different models have been developed to account for various aging phenomena, including parasitic side reactions [23], solid electrolyte interface formation [27], and resistance increase [28]. The work in [29] estimates the capacity loss in LiFePO₄ batteries by an Arrhenius type of model, which had been previously introduced in [27]:

$$\nabla Q = B \times e^{-\left(\frac{E_a}{R \cdot T}\right)} \cdot Ah^z \quad (12)$$

where ∇Q is the percentage of capacity loss, B is a pre-exponential factor, E_a [$\text{J} \cdot \text{mol}^{-1}$] is the activation energy from Arrhenius, $R = 8.314$ [$\text{J} \cdot \text{mol}^{-1} \cdot \text{K}^{-1}$] is the gas constant, T is the absolute temperature, $z \approx 0.55$ is the power law factor, and Ah is the Ah-throughput:

$$Ah = n \times DoD \cdot Q_{MAX} \quad (13)$$

with n and DoD being the number of cycles and the depth of discharge, respectively. For analytical purposes, the authors of [29] propose a linearized form of Equation (13):

$$\text{Ln}(\nabla Q) = \text{Ln}(B) - \left(\frac{E_a}{R \cdot T}\right) + z \times \text{Ln}(Ah) \quad (14)$$

This linearized form makes it handfull to calculate the coefficients B , E_a , and z from experimental data. This is typically done by means of a multi-dimensional regression analysis, which takes multiple capacity curves for different current rates and temperatures into account [30].

The authors of [29] also provide an expression for the activation energy E_a as a function of the current rate C_{rate} based on experimental results for LiFePO₄:

$$E_a(C_{rate}) = 31500 - 370.3 \times C_{rate} \quad (15)$$

Finally, they provide data to calculate the pre-exponential factor B , although a general expression is not given as with E_a . Fortunately, this was recently done in another work by different authors [31], deriving the following:

$$\text{Ln}(B) = 1.226 \times e^{-0.2797 \cdot C_{rate}} + 9.263 \quad (16)$$

Hence, B can be dynamically estimated under different battery current profiles and current rates by means of Equation (16), as discussed later.

Although the aging model originally proposed in [29] was intended for constant C_{rate} cycling, the work presented in [31] suggests that it can also be used for cycle life estimation under non-uniform current profiles.

The battery aging model described in this work does not consider calendar ageing, nor Depth of Discharge (DoD) influence, i.e., 1 Ah discharge implies the same capacity loss along the whole SoC range.

The battery model data used in the application example (Section 4) are obtained from the datasheet of a commercial A123 lithium iron phosphate ($LiFePO_4$), 3.3 V, 2.3 Ah cell [32], which is used for all the simulations and analyses performed during this paper. The runtime, thermal, and aging models that conform to the complete battery model used in this work are validated by comparison with the manufacturer's datasheet in [33]. Figure 2 illustrates the aging model validation.

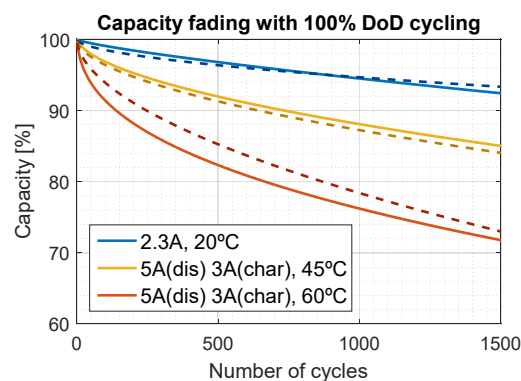


Figure 2. Comparison between the battery model implemented in this work and the manufacture's datasheet: capacity loss due to cycling. Dashed curves are those obtained with the model [33].

3.2. EDLC Model

The EDLC model is obtained from Mathworks in the SimPower toolbox of Simulink [34]. This model is analytical (no look-up tables are needed), non-linear, takes self-discharge into account, expresses the output voltage using a Stern equation, and is experimentally validated in [35].

A commercial EDLC cell from Maxwell Technologies (San Diego, CA, USA) was used for all the simulations and analyses performed (Section 4). Namely, a 2.7V 310F EDLC was chosen [36].

Temperature dependence has not been included in the EDLCs model for three reasons. First, it is not particularly relevant for the purposes of this study (for instance, the aging of EDLCs is not assessed). Secondly, EDLCs are less sensitive to temperature than batteries. Thirdly, it was assumed that temperature rises in batteries were larger than in EDLCs.

3.3. DC-DC Converter Power Losses

The topology used for this study is a buck-boost interleaved IGBTs DC-DC converter [37]. The interleaving technique connects DC-DC converters in parallel to split the current flow between two or to create more conversion stages, providing a lag between the pulse-width modulation (PWM) control signals of each converter stage. Its main advantages are constant switching frequency, current ripple reduction, and capacitor and inductor size/weight shrinkage. Higher energy efficiency is also expected from interleaved DC-DC converters when compared to conventional buck-boost converters [38].

Conduction losses [37], IGBTs switching losses [39], and diode turn-off losses are calculated for a constant switching frequency of 5 kHz. Constant losses (control, drivers, and cooling) are not considered.

3.4. Vehicle Model

In order to calculate the power demanded by the load (drive), P_{HESS} , the following equations need to be applied:

$$P_{HESS}(t) = T_{em} \frac{\omega_{mec}}{\eta_{DRIVE}} (\text{traction mode}) \quad (17)$$

$$P_{HESS} = T_{em} \times \omega_{mec} \times \eta_{DRIVE} (\text{regenerative mode})$$

where η_{DRIVE} is the average efficiency of the drive (inverter + machine) and T_{em} is the electromagnetic torque provided by the traction motor, given by:

$$T_{em} - T_{load} = J \times \frac{d\omega_{mec}}{dt} + B \cdot \omega_{mec} \quad (18)$$

$$J = J_{high} + \frac{J_{low}}{i_{GEAR}^2} + M \frac{ERR^2}{i_{GEAR}^2} \quad (19)$$

$$T_{load} = \frac{ERR}{i_{GEAR} \cdot \eta_{GEAR}} F_T (\text{traction mode}) \quad (20)$$

$$T_{load} = \frac{ERR \cdot \eta_{GEAR}}{i_{GEAR}} F_T (\text{regenerative mode})$$

where $ERR [m]$ is the effective rolling radius (which is not the same as the loaded tire radius [40]), $i_{GEAR} [-]$ is the transmission gear ratio, $\eta_{GEAR} [-]$ is the transmission energy efficiency (assumed to be constant and equal to 0.96 [41]), and J is the total inertia. J_{high} and J_{low} are the total rotatory inertia in the high speed shaft (motor shaft) and in the low speed shaft (wheels shaft), respectively. Most of the vehicle inertia is given by its mass M .

3.5. Control Strategy

There are two main groups of control strategies to be potentially selected: those based on rules and those based on advanced control techniques. For instance, a comparison of four rule-based energy management strategies is presented in [42]. On the other hand, advanced control strategies include predictive control algorithms capable of determining a power-mix in real time, based on the expected load demand and loss models for all system components [9] or aiming at the optimization of the system's performance [43].

Topology 2 allows several control possibilities since the DC-DC converter does not have to control the DC-link voltage U_{DC} , which is fixed by batteries. Due to this restricted flexibility and although advanced control techniques could be explored, the most straightforward way to control the system is with a technique based on rules [11].

The algorithm implemented in this work behaves as follows:

- A. While motoring, the power demanded by the drive, P_{dem} , is evaluated, and a certain value of P_{MIN} is defined for the batteries, depending on their technology. Two main cases are distinguished:
 1. If the power demanded by the drive is low, $P_{dem} < P_{MIN}$, then the batteries provide all the traction power. Two sub-cases are considered depending on the EDLC voltage and the vehicle speed:
 - If $EDLC \text{ SoC} > SoC_{min}$, the EDLCs remain disabled.
 - If $EDLC \text{ SoC} < SoC_{min}$, the batteries also provide power (up to a given value P_{Ch}) to recharge the EDLCs until they reach their minimum value.
 2. If the power demanded by the drive is high $P_{dem} > P_{MIN}$, the EDLCs provide all the power but P_{MIN} , which is given by the batteries.
- B. While regeneratively braking, EDLCs absorb as much power as possible. Once they are fully charged, the batteries absorb as much power as possible. Finally, conventional brakes deal with the remaining power.

Obviously, the EDLCs' SoC can overrule any of the above rules so that the batteries will take care of any power that cannot be handled by them. In extreme situations (completely full or empty EDLCs), this implies that the HESS will temporarily behave like a conventional ESS.

4. HESS Design Methodology and Application Example

4.1. HESS Design Methodology

There are not many papers comparing HESS in terms of energy efficiency, especially when considering different hybridization grades. This 'hybridization grade' concept refers to the proportion between the energy density storage (batteries) and the power density storage (EDLCs). In this work, the hybridization grade is quantified by means of a magnitude called "hybridization percentage", *HybPer*, which express the proportion between the EDLCs' weight, W_{EDLC} , referring to the total ESS weight (power converters not included), and W_{BAT} , the weight of batteries:

$$HybPer = \frac{W_{EDLC}}{W_{EDLC} + W_{BAT}} \quad (21)$$

The HESS design methodology proposed in this paper, which aims at finding the most suitable *HybPer* regarding HESS efficiency and battery aging, can be described as a 'brute-force' optimization methodology. Considering that there are two variables to optimize (HESS efficiency and battery aging) and one design variable (*HybPer*), this methodology is adequate since the complexity of the problem and the number of cases do not justify the use of a more complex method. Applying a more intelligent optimization methodology does not guarantee reaching a better optimum. The proposed methodology is described in the following steps:

Step 1. Select the hybrid storage technologies, power electronics topology, and control strategy to be operated. A complex topology should not be chosen if the control does not match the topology complexity.

Step 2. Define one or several operation scenarios. In this case, one or several driving cycles.

Step 3. Define the P_{MIN} value for the batteries. This parameter will depend on the technology and most of the time will follow the manufacturer's recommendations.

Step 4. Complete models introducing data corresponding to the particular selected storage devices and vehicle: models of the battery, EDLCs, DC-DC converter, and EB model described in Section 3 must be completed with data obtained from the HESS designer battery, EDLCs, and DC-DC converter choice, together with the selected EB parameters and driving cycles.

Step 5. Perform simulations: an analysis of the complete model must be performed, increasing *HybPer* in each simulation and measuring HESS efficiency and capacity fade, as explained in Section 3, so both characteristic curves are obtained. If several controls are suitable for implementation, Step 5 should be performed for every control.

Step 6. Combine results in order to find the best *HybPer* for the HESS design: in order to find the most suitable solution, the results obtained from the performance study should be finally combined in a result function, in which, depending on the relative weight given to the two measurable variables (efficiency and battery capacity fade), a *HybPer* can be obtained.

4.2. Application Example

In order to present how the methodology described in the previous section is applied to a real case, the case study of a Castrosua Tempus Hybrid bus, the characteristics of which are presented in Table 2, has been chosen for analysis.

Table 2. Castrosua Tempus Hybrid Parameters.

Model Parameters			
Energy	80 kWh	Weight	17,000 kg
Nominal V	666 V	Wheel radius	505.7 mm
Nominal C	117 Ah	Height	4 m
C_D	0.5	Width	2.5 m
C_F	0.055	Gear reduction	17.65

The same structure of steps as in Section 4.1 will be followed.

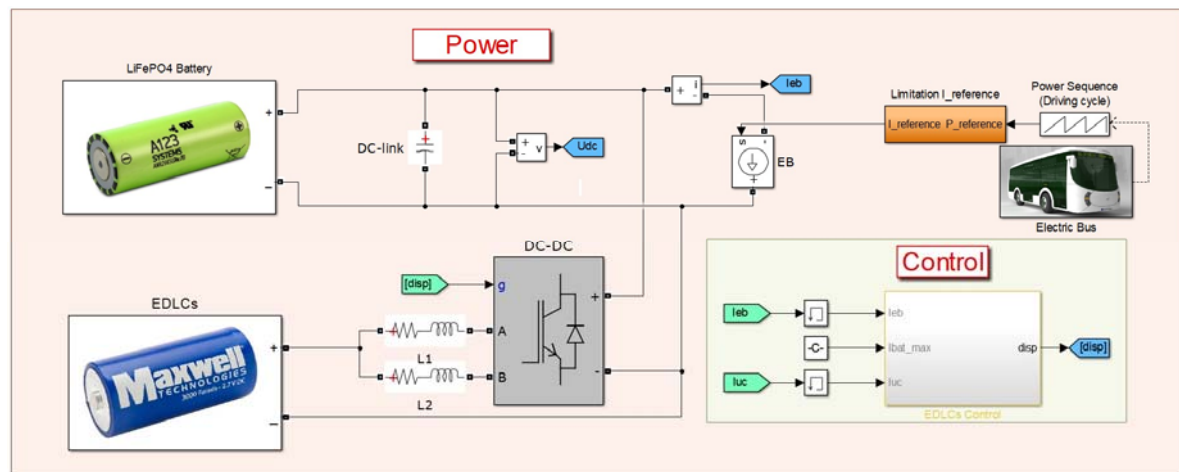
Step 1. The Li-batteries and EDLC are defining the HESS. As has been previously introduced, Topology 2 has been selected as the most reliable solution, together with the control described in Section 3.5.

Step 2. Different driving cycles have been defined in this example for comparison. The first driving cycle used in this work is one of the ARTEMIS European driving cycles [44]. These cycles were built-up to be representative of the actual conditions of vehicle usage and to reproduce the diversity of the observed driving conditions. Such driving cycles present a real advantage as they are derived from a large database. The chosen cycle consists of two consecutive ARTEMIS urban cycles, with a total duration of 36 min in flat terrain. The net energy consumption is 34 kWh. The second driving cycle used in this work is the Economic Commission for Europe ECE-15 (Urban Driving Cycle) of the New European Driving Cycle (NEDC) [45]. Although it does not represent real driving conditions, NEDC is still used as a standard driving cycle for testing vehicle emissions. The chosen cycle is a 26-min driving cycle, consisting of two consecutive NEDC urban cycles with a net energy consumption of 28 kWh.

Step 3. Three different values of P_{MIN} have been chosen for the control strategy: 1C, 3C, and 5C.

Step 4. Battery and EDLCs data, as mentioned, were obtained from [32,36].

Step 5. Simulink SimPowerSystem has been used for performing the simulation studies. Figure 3 shows the general block diagram containing all the different HESS components and the selected EB and cycle power profile.

**Figure 3.** Matlab Simulink SimPowerSystem simulation model developed for the performed study.

From the simulation analysis accomplished, several discussions will follow.

The HESS global energy efficiencies (batteries, EDLCs, and DC-DC converters) for the ARTEMIS cycle for three different values of P_{MIN} (1C, 3C, and 5C) are displayed in Figure 4, whereas the capacity fade after 1000 cycles for the same three cases is illustrated in Figure 5. The figures include mean tendency lines for each value of P_{MIN} .

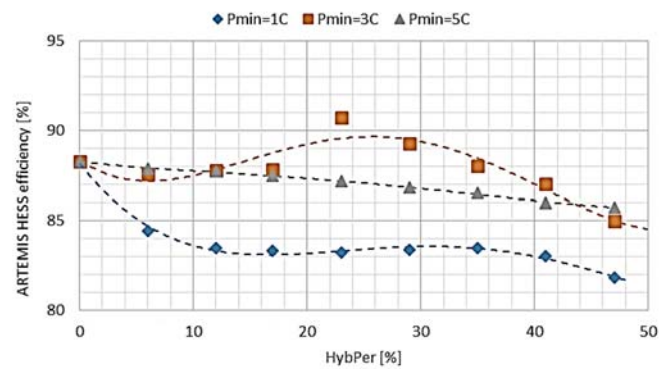


Figure 4. HESS global efficiency for topology 2 as a function of the hybridization percentage for three different values of P_{MIN} .

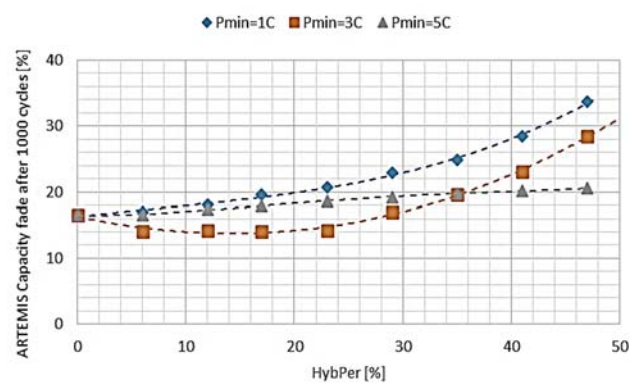


Figure 5. Battery aging for topology 2 as a function of the hybridization percentage for three different values of P_{MIN} .

Both figures state that a P_{MIN} value of 3C allows the EB to work with a higher efficiency and lower battery aging, showing a maximum efficiency value for a certain $HybPer$ when applied to the specified topology and studied driving cycle.

It is noticeable that the battery capacity fade is relevant after 1000 cycles. This happens due to the specific relationship between the chosen battery size and the driving cycle, which forces the battery to work with high C_{rate} (above P_{MIN}) once the EDLCs are discharged.

The energy efficiency results are shown in Figure 6 for topology 2 for the ARTEMIS cycle, with the most efficient control ($P_{MIN} = 3C$).

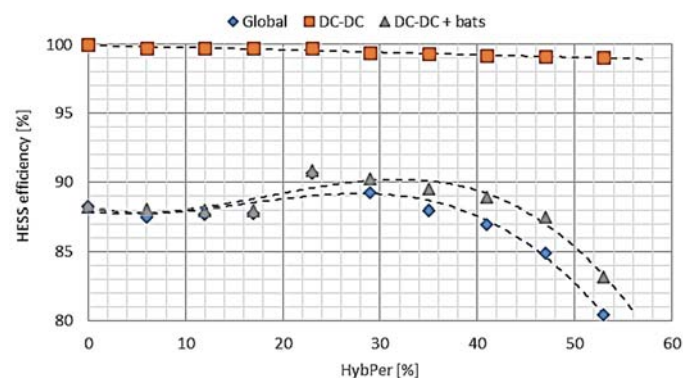


Figure 6. DC-DC, DC-DC and Battery, and HESS global efficiency for topology 2 ($P_{MIN} = 3C$) as a function of the hybridization percentage.

The value marked with \blacklozenge is the HESS global efficiency. For low hybridization percentages (0% to 30%), more *HybPer* implies higher efficiency. However, it strongly decreases after reaching its maximum. The curve marked with \blacksquare is the efficiency of the DC-DC converter. As *HybPer* increases (as batteries are replaced by EDLCs, keeping the total weight constant), the converter handles more current, and its average efficiency decreases. Finally, the value marked with \blacktriangle is the DC-DC and batteries efficiency. Obviously, for *HybPer* = 0%, this value matches the global efficiency since there are no EDLCs, but then, after the maximum efficiency point, it follows a similar tendency as the global efficiency, although keeping its value slightly higher due to the non-influence of the drop in the efficiency of EDLCs.

In order to illustrate the driving cycle dependency for the analysis proposed in this paper, Figure 7 compares the global HESS energy efficiency for ARTEMIS and NEDC driving cycles with the same control strategy implemented ($P_{MIN} = 3C$). The HESS efficiency improves for both driving cycles compared to a conventional ESS (*HybPer* = 0), reaching their maximum efficiency values at different *HybPer*.

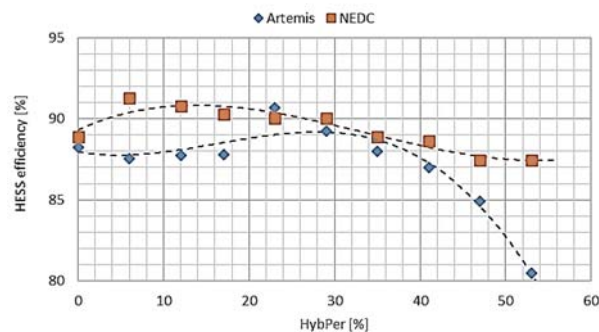


Figure 7. HESS global efficiency for topology 2 as a function of the hybridization percentage for two different driving cycles.

The SoC of the HESS at the end of the ARTEMIS driving cycle is depicted in Figure 8. It is clear that replacing batteries with EDLCs while keeping the weight constant will severely impact the EB range. Figure 8 shows this reduction to the point that the driving cycle cannot be finished with *HybPer* $\geq 53\%$.

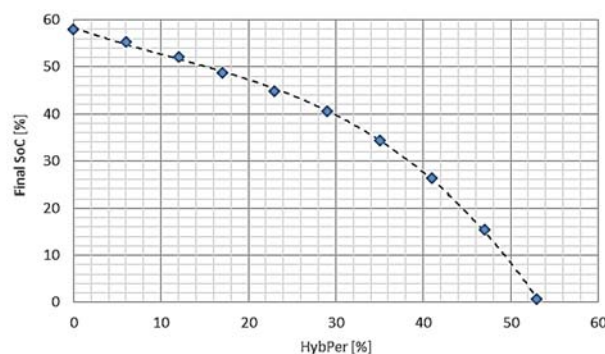


Figure 8. Global state of change (SoC) (batteries and EDLCs) for topology 2 as a function of the hybridization percentage at the end of the ARTEMIS cycle.

Regarding battery aging, Figure 9 shows the capacity loss for different *HybPer* values and for the two driving cycles considered ($P_{MIN} = 3C$). 1000 cycles are considered for the ARTEMIS cycle, while, for the NEDC cycle, the number of cycles is 121, in order to measure the capacity fade after dealing with the same amount of energy.

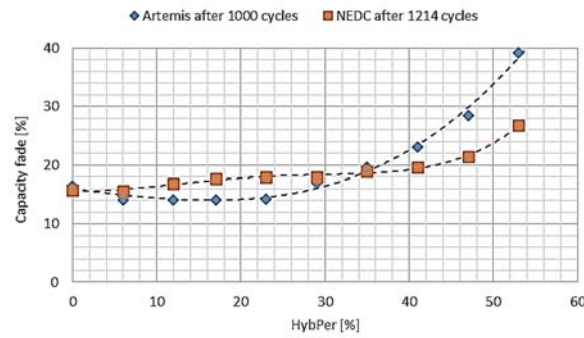


Figure 9. The battery aging for topology 2 as a function of the hybridization percentage for two different driving cycles.

Figure 9 states that there is a considerable difference between both driving cycles when *HybPer* is below 10% and above 30%. It is noticeable that the capacity fade tendency follows the HESS efficiency, decreasing when the HESS efficiency grows. However, the minimum capacity fade does not necessarily match the maximum HESS efficiency at the same *HybPer* point, e.g., for the ARTEMIS cycle, the minimum capacity fade is obtained with a *HybPer* of 17% and the maximum HESS efficiency with 23%, while, for the NEDC cycle, the most suitable *HybPer* is 6%, which minimizes the capacity fade and maximizes the efficiency.

As illustrated with the application example presented in this section, every HESS designer would need to follow the described methodology, running the simulation models after introducing the particular information (type of batteries, EDLCs, DC-DC converter, EB type, or driving cycle) according to the case of study.

Lastly, in order to find the most suitable solution for both HESS designers and companies operating EB fleets, the results obtained from this study should be combined in a result function. HESS designers, according to the price and availability of battery replacements, the price of the saved energy, the price of EDLCs, etc. together with other circumstances that may occur, should weight the two measurable variables (HESS efficiency and battery aging), i.e., they should establish the importance they give to each variable so the following result function can be used:

$$y = Weight_1 \cdot (\text{HESS Eff curve}) + Weight_2 \cdot (C \text{ fade curve}) \quad (22)$$

where y is the result curve, $Weight_1$ is the relative importance of the HESS efficiency, $Weight_2$ is the relative importance of the capacity fade, $HESS - Eff \text{ curve}$ is the HESS efficiency tendency curve, and $C - fade \text{ curve}$ is the capacity fade tendency curve.

In order to find the *HybPer* that minimizes cost, the derivative of cost with respect to *HybPer* needs to be equal to zero.

Taking the ARTEMIS cycle as an example, and with $Weight_1 = Weight_2 = 1$ (both variables are equally important), the result of Equation (22) is as follows:

$$y = (-0.000232x^3 + 0.011337x^2 - 0.092284x + 87.967338) + (-0.000219x^3 + 0.000430x^2 + 0.167186x + 84.069359) \quad (23)$$

where $x = HybPer$. Finally:

$$\frac{dy}{dx} = 0 \Rightarrow HybPer = 20.1423\% \quad (24)$$

As has been previously indicated, for the ARTEMIS cycle, the minimum capacity fade is obtained with a *HybPer* of 17%, and the maximum HESS efficiency with 23%, so the obtained *HybPer* is located between both values. It is expected that, changing the variable weights, this *HybPer* will move towards values that improve the behavior of the most important variable. In this case study, changing the HESS

efficiency weight to two, while keeping the battery capacity fade weight equal to one, the following result is obtained:

$$\frac{dy}{dx} = 0 \Rightarrow HybPer = 22.1688\% \quad (25)$$

5. Conclusions

This paper presents an approach to HESS dimensioning that considers all its components and focuses on the hybridization percentage when weight constraints are taken into consideration since it is not obvious how many EDLCs a HESS should contain (or even if the ESS should contain any EDLCs at all). The proposed study has potential interest for HESS designers, EB manufacturers, and companies operating EB fleets.

A HESS dimensioning methodology has been proposed, attending to two different criteria: global efficiency (batteries, EDLCs, and DC-DC converters) and battery capacity fade. Simulation models for EDLCs, DC-DC converters, and batteries are described and implemented, with improvements in the latter regarding battery cell and battery pack temperature dependency and resistance modelling. The Li-ion battery model presented in this paper improves accuracy without a substantial increase in complexity.

In order to demonstrate how to implement the proposed methodology, as well as to analyse the results arose from it, the most studied HESS topology is considered as an example (topology 2), together with a specific rule-based control strategy, for two different driving cycles (ARTEMIS and NEDC).

The results show that there is a different hybridization percentage that maximizes HESS global efficiency and minimizes capacity fade for the ARTEMIS and NEDC cycles, which suggests that there is a most advantageous hybridization percentage for each topology, control strategy, and driving cycle, as has been illustrated by the example case presented in this paper. It is important to notice that increasing the hybridization percentage, i.e., increasing the weight of the EDLCs while decreasing that of the batteries, has a huge influence on the driving range, reducing it considerably.

It is also true that, in order to find the most suitable solution, the whole range of HESS and control alternatives have to be considered for a specified cycle, although control strategies are usually developed for a specific HESS topology. This implies that, when designing a HESS and once the EB cycle is known, the HESS topology should be chosen depending on the control strategy that the designer is able to provide so that the hardware complexity matches the software complexity.

HESS designers should perform a study like the one proposed in this work in order to find the most suitable solution for their specific application, which should include, in the final stage, a translation to economical terms for maximizing benefits.

Acknowledgments: This work was partially supported by the following research projects: ‘PCBBUS. Plan Nacional 2014—Proyectos de I+D+I. Reference: TRA2014-57520-R’ and ‘SEGVAUTO-TRIES-CM. Convocatoria de Programas de I+D en Tecnología/2013 Orden 3017/2014 del 24 de septiembre, B.O.C.M. Núm. 252 del 23 de octubre de 2014. Reference: S2013/MIT-2713’.

Author Contributions: Jorge Nájera, Pablo Moreno-Torres, and Jaime R. Arribas conceived and designed the paper; Jorge Nájera and Pablo Moreno-Torres performed and analyzed the simulation studies; Jorge Nájera and Pablo Moreno-Torres wrote the paper; and Marcos Lafoz, Rosa María de Castro, and Jaime Rodríguez Arribas reviewed and rearranged the paper.

Conflicts of Interest: The authors declare no conflicts of interest.

References

1. EPA. Sources of Greenhouse Gas Emissions. Available online: <https://www.epa.gov/ghgemissions/sources-greenhouse-gas-emissions> (accessed on 20 December 2016).
2. Transport–Horizon 2020–European Commission. Available online: <https://ec.europa.eu/programmes/horizon2020/en/area/transport> (accessed on 12 September 2017).

3. Fiona Harvey Environment Correspondent. Four of world's biggest cities to ban diesel cars from their centres. *Guardian* **2016**. Available online: www.theguardian.com/environment/2016/dec/02/four-of-worlds-biggest-cities-to-ban-diesel-cars-from-their-centres (accessed on 20 August 2017).
4. Lukic, S.M.; Cao, J.; Bansal, R.C.; Rodriguez, F.; Emadi, A. Energy Storage Systems for Automotive Applications. *IEEE Trans. Ind. Electron.* **2008**, *55*, 2258–2267. [[CrossRef](#)]
5. Khaligh, A.; Li, Z. Battery, Ultracapacitor, Fuel Cell, and Hybrid Energy Storage Systems for Electric, Hybrid Electric, Fuel Cell, and Plug-In Hybrid Electric Vehicles: State of the Art. *IEEE Trans. Veh. Technol.* **2010**, *59*, 2806–2814. [[CrossRef](#)]
6. Ren, G.; Ma, G.; Cong, N. Review of electrical energy storage system for vehicular applications. *Renew. Sustain. Energy Rev.* **2015**, *41*, 225–236. [[CrossRef](#)]
7. Lukic, S.M.; Wirasingha, S.G.; Rodriguez, F.; Cao, J.; Emadi, A. Power Management of an Ultracapacitor/Battery Hybrid Energy Storage System in an HEV. In Proceedings of the 2006 IEEE Vehicle Power and Propulsion Conference, Windsor, UK, 6–8 September 2006; pp. 1–6.
8. Cao, J.; Emadi, A. A New Battery/UltraCapacitor Hybrid Energy Storage System for Electric, Hybrid, and Plug-In Hybrid Electric Vehicles. *IEEE Trans. Power Electron.* **2012**, *27*, 122–132. [[CrossRef](#)]
9. Laldin, O.; Moshirvaziri, M.; Trescases, O. Predictive Algorithm for Optimizing Power Flow in Hybrid Ultracapacitor/Battery Storage Systems for Light Electric Vehicles. *IEEE Trans. Power Electron.* **2013**, *28*, 3882–3895. [[CrossRef](#)]
10. Gao, L.; Dougal, R.A.; Liu, S. Power enhancement of an actively controlled battery/ultracapacitor hybrid. *IEEE Trans. Power Electron.* **2005**, *20*, 236–243. [[CrossRef](#)]
11. Carter, R.; Cruden, A.; Hall, P.J. Optimizing for Efficiency or Battery Life in a Battery/Supercapacitor Electric Vehicle. *IEEE Trans. Veh. Technol.* **2012**, *61*, 1526–1533. [[CrossRef](#)]
12. Amjadi, Z.; Williamson, S.S. A Novel Control Technique for a Switched-Capacitor-Converter-Based Hybrid Electric Vehicle Energy Storage System. *IEEE Trans. Ind. Electron.* **2010**, *57*, 926–934. [[CrossRef](#)]
13. Kohler, T.P.; Buecherl, D.; Herzog, H.G. Investigation of control strategies for hybrid energy storage systems in hybrid electric vehicles. In Proceedings of the 2009 IEEE Vehicle Power and Propulsion Conference, Dearborn, MI, USA, 7–10 September 2009; pp. 1687–1693.
14. Moreno-Torres, P.; Navarro, G.; Blanco, M.; Lafoz, M. Multifunctional test bench for the emulation and testing of electric vehicle fast-charging from urban railway power lines. In Proceedings of the 2015 IEEE International Conference on Industrial Technology (ICIT), Seville, Spain, 17–19 March 2015; pp. 1081–1087.
15. Grbović, P. Energy Storage Technologies and Devices. In *Ultra-Capacitors in Power Conversion Systems*; John Wiley & Sons, Ltd.: Chichester, UK, 2013; pp. 1–21. ISBN 978-1-118-69363-6.
16. Implement Generic Battery Model–Simulink–MathWorks España. Available online: <https://es.mathworks.com/help/physmod/sps/powersys/ref/battery.html;jsessionid=1408413e56d376608b781f4f079a> (accessed on 8 September 2017).
17. Shepherd, C.M. Design of Primary and Secondary Cells II. An Equation Describing Battery Discharge. *J. Electrochem. Soc.* **1965**, *112*, 657–664. [[CrossRef](#)]
18. Tremblay, O.; Dessaint, L.A.; Dekkiche, A.I. A Generic Battery Model for the Dynamic Simulation of Hybrid Electric Vehicles. In Proceedings of the 2007 IEEE Vehicle Power and Propulsion Conference, Arlington, TX, USA, 9–12 September 2007; pp. 284–289.
19. Tremblay, O.; Dessaint, L.A. Experimental Validation of a Battery Dynamic Model for EV Applications. *World Electr. Veh. J.* **2009**, *3*, 289–298.
20. Chen, M.; Rincon-Mora, G.A. Accurate electrical battery model capable of predicting runtime and I-V performance. *IEEE Trans. Energy Convers.* **2006**, *21*, 504–511. [[CrossRef](#)]
21. Saw, L.H.; Somasundaram, K.; Ye, Y.; Tay, A.A.O. Electro-thermal analysis of Lithium Iron Phosphate battery for electric vehicles. *J. Power Sources* **2014**, *249*, 231–238. [[CrossRef](#)]
22. Chen, Y.; Evans, J.W. Three-Dimensional Thermal Modeling of Lithium-Polymer Batteries under Galvanostatic Discharge and Dynamic Power Profile. *J. Electrochem. Soc.* **1994**, *141*, 2947–2955. [[CrossRef](#)]
23. Forgez, C.; Vinh Do, D.; Friedrich, G.; Morcrette, M.; Delacourt, C. Thermal modeling of a cylindrical LiFePO₄/graphite lithium-ion battery. *J. Power Sources* **2010**, *195*, 2961–2968. [[CrossRef](#)]
24. Ye, Y.; Shi, Y.; Cai, N.; Lee, J.; He, X. Electro-thermal modeling and experimental validation for lithium ion battery. *J. Power Sources* **2012**, *199*, 227–238. [[CrossRef](#)]

25. Rao, L. Heat-Generation Rate and General Energy Balance for Insertion Battery Systems. *J. Electrochem. Soc.* **1997**, *144*, 2697. [CrossRef]
26. Zhu, C.; Li, X.; Song, L.; Xiang, L. Development of a theoretically based thermal model for lithium ion battery pack. *J. Power Sources* **2013**, *223*, 155–164. [CrossRef]
27. Spotnitz, R. Simulation of capacity fade in lithium-ion batteries. *J. Power Sources* **2003**, *113*, 72–80. [CrossRef]
28. Dubarry, M.; Svoboda, V.; Hwu, R.; Liaw, B.Y. Capacity loss in rechargeable lithium cells during cycle life testing: The importance of determining state-of-charge. *J. Power Sources* **2007**, *174*, 1121–1125. [CrossRef]
29. Wang, J.; Liu, P.; Hicks-Garner, J.; Sherman, E.; Soukiazian, S.; Verbrugge, M.; Tataria, H.; Musser, J.; Finamore, P. Cycle-life model for graphite-LiFePO₄ cells. *J. Power Sources* **2011**, *196*, 3942–3948. [CrossRef]
30. Petricca, M.; Shin, D.; Bocca, A.; Macii, A.; Macii, E.; Poncino, M. Automated generation of battery aging models from datasheets. In Proceedings of the 2014 IEEE 32nd International Conference on Computer Design (ICCD), Seoul, Korea, 19–22 October 2014; pp. 483–488.
31. Shen, J.; Dusmez, S.; Khaligh, A. Optimization of Sizing and Battery Cycle Life in Battery/Ultracapacitor Hybrid Energy Storage Systems for Electric Vehicle Applications. *IEEE Trans. Ind. Inf.* **2014**, *10*, 2112–2121. [CrossRef]
32. A123 Systems High Power Lithium Ion Cell ANR26650M1. 2006. Available online: www.a123systems.com/Collateral/Documents/English-US/A123%20Systems%20ANR26650%20Data%20Sheet.pdf (accessed on 15 June 2017).
33. Moreno-Torres, P. *Analysis and Design Considerations of an Electric Vehicle Powertrain Regarding Energy Efficiency and Magnetic Field Exposure*; Universidad Politécnica de Madrid: Madrid, Spain, 2016.
34. Implement Generic Supercapacitor Model–Simulink–MathWorks España. Available online: <http://es.mathworks.com/help/physmod/sps/powersys/ref/supercapacitor.html> (accessed on 20 December 2016).
35. Bland, P.C. Développement d'un Modèle de Simulation de Supercondensateur et Validation Expérimentale. Master's Thesis, École de Technologie Supérieure, Montreal, QC, Canada, 2012.
36. Maxwell Technologies Ultracapacitors (Document Number: 3000489.1). 2014. Available online: www.maxwell.com/images/documents/PI_maxwell_technologies_product_comparison_matrix.pdf (accessed on 15 June 2017).
37. Grbović, P. Interface DC–DC Converters. In *Ultra-Capacitors in Power Conversion Systems*; John Wiley & Sons, Ltd.: Chichester, UK, 2013; pp. 216–315. ISBN 978-1-118-69363-6.
38. Arango, E.; Ramos-Paja, C.; Calvente, J.; Giral, R.; Serna, S. Asymmetrical Interleaved DC/DC Switching Converters for Photovoltaic and Fuel Cell Applications—Part 1: Circuit Generation, Analysis and Design. *Energies* **2012**, *5*, 4590–4623. [CrossRef]
39. ABB Switzerland Ltd. Thermal Runaway during Blocking (Application Note 5SYA 2045-01) 2013. Available online: www.5dcomponents.com/pdf/5SYA-2045-01-thermal-runaway-during-blocking.pdf (accessed on 23 June 2017).
40. Pacejka, H.B. *Tyre and Vehicle Dynamics*, 2nd ed.; Butterworth-Heinemann: Oxford, UK, 2006; ISBN 978-0-7506-6918-4.
41. Ehsani, M.; Gao, Y.; Emadi, A. *Modern Electric, Hybrid Electric, and Fuel Cell Vehicles Fundamentals, Theory, and Design*; CRC Press: Boca Raton, FL, USA, 2010; ISBN 978-1-4200-5400-2.
42. Allègre, A.L.; Trigui, R.; Bouscayrol, A. Different energy management strategies of Hybrid Energy Storage System (HESS) using batteries and supercapacitors for vehicular applications. In Proceedings of the 2010 IEEE Vehicle Power and Propulsion Conference, Lille, France, 1–3 September 2010; pp. 1–6.
43. Zhou, F.; Xiao, F.; Chang, C.; Shao, Y.; Song, C. Adaptive Model Predictive Control-Based Energy Management for Semi-Active Hybrid Energy Storage Systems on Electric Vehicles. *Energies* **2017**, *10*, 1063. [CrossRef]
44. André, M. The ARTEMIS European driving cycles for measuring car pollutant emissions. *Sci. Total Environ.* **2004**, *334*–*335*, 73–84. [CrossRef] [PubMed]
45. Giakoumis, E.G.; Zachiotis, A.T. Investigation of a Diesel-Engined Vehicle's Performance and Emissions during the WLTC Driving Cycle—Comparison with the NEDC. *Energies* **2017**, *10*, 240. [CrossRef]

